Electronic Supplementary Material (ESI) for Journal of Materials Chemistry A.

SUPPLIMENTARY INFORMATION

Underwater Magneto Driven Air De-bubbler

Udara Bimendra Gunatilake[1,2], Yara Alvarez-Braña[1,2], Edilberto Ojeda[1,2], Lourdes Basabe-Desmonts[2,3,4,5,*], Fernando Benito-Lopez[1,4,5,*]

[1]*Microfluidics Cluster UPV/EHU, Analytical Microsystems & Materials for Lab-on-a-Chip Group, Analytical Chemistry Department, University of the Basque Country UPV/EHU, Spain*

[2]*Microfluidics Cluster UPV/EHU, BIOMICs microfluidics Group, Lascaray Research Center, University of the Basque Country UPV/EHU, Vitoria-Gasteiz, Spain*

[3]*IKERBASQUE, Basque Foundation for Science, Bilbao, Spain*

[4]*Bioaraba Health Research Institute, Microfluidics Cluster UPV/EHU, Vitoria-Gasteiz, Spain*

[5]*BCMaterials, Basque Centre for Materials, Micro and Nanodevices, UPV/EHU Science Park, Leioa, Spain*

SI-1 Fabrication of the microfluidic device

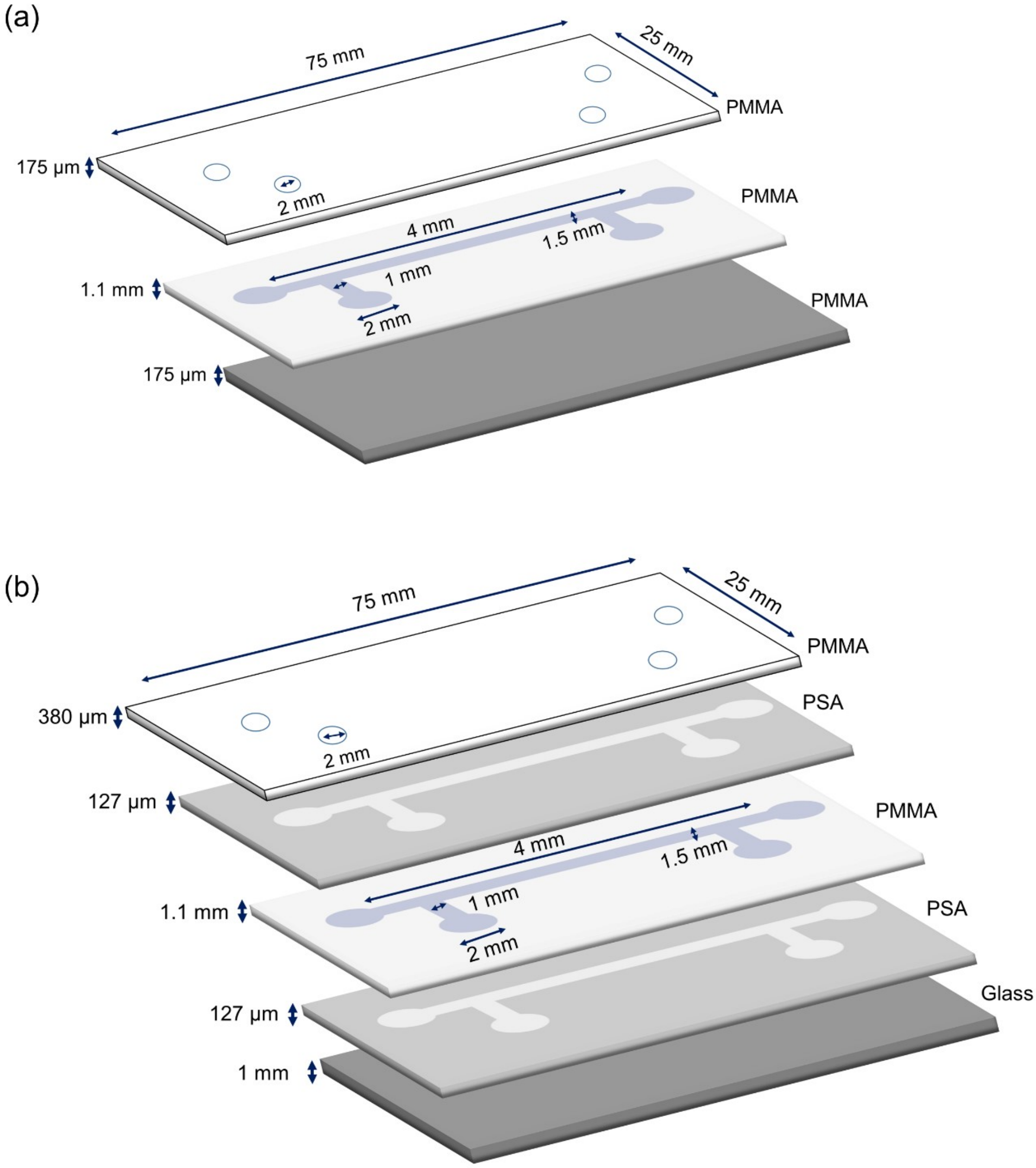

Figure SI-1: Dimensions and materials of the microfluidic devices with (a) PMMA bottom and (b) glass bottom surfaces.

SI-2 Characterisation of the SMPs

The FTIR spectra of bare Fe and SMPs (C_8-Fe) was analysed to check the modification of the octyl hydrocarbon chain on the Fe surface. As depicted in Figure SI-2 (C_8-Fe), the high intense distinguish peaks frequency at 2850, 2941, and 2965 cm^{-1} are due to the stretching vibrations of CH_2 in alkyl chains.[1] The peak at 1460 cm^{-1} can be attributed to the CH_2 bending vibrational peak of the coated molecules. As well, the stretching vibrational peaks at 866, 990 and 1115 cm^{-1} in the SMPs spectrum were assigned to Si-C, Si-O-Fe and Si-O bonds respectively, demonstrating the binding of the alkyl chain through the silane group to the particles surface. The common peaks of residual water OH stretching and bending were found in both Fe and SMPs at the positions of 3430/3340 cm^{-1} and 1630/1660 cm^{-1}.[1–4] However, the intensity of the O-H peaks was reduced in the SMPs spectrum due to the hydrophobic alkyl groups, inhibiting the absorption of residual water to the surface of the Fe particle.

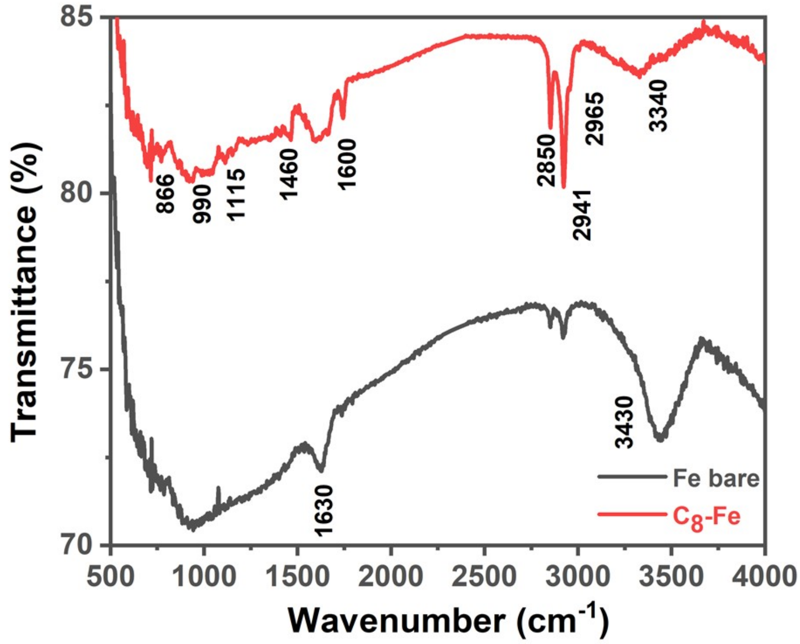

Figure SI-2: FTIR spectra of bare Fe microparticles (black spectrum) and the chemically modified SMPs (C_8-Fe) (red spectrum).

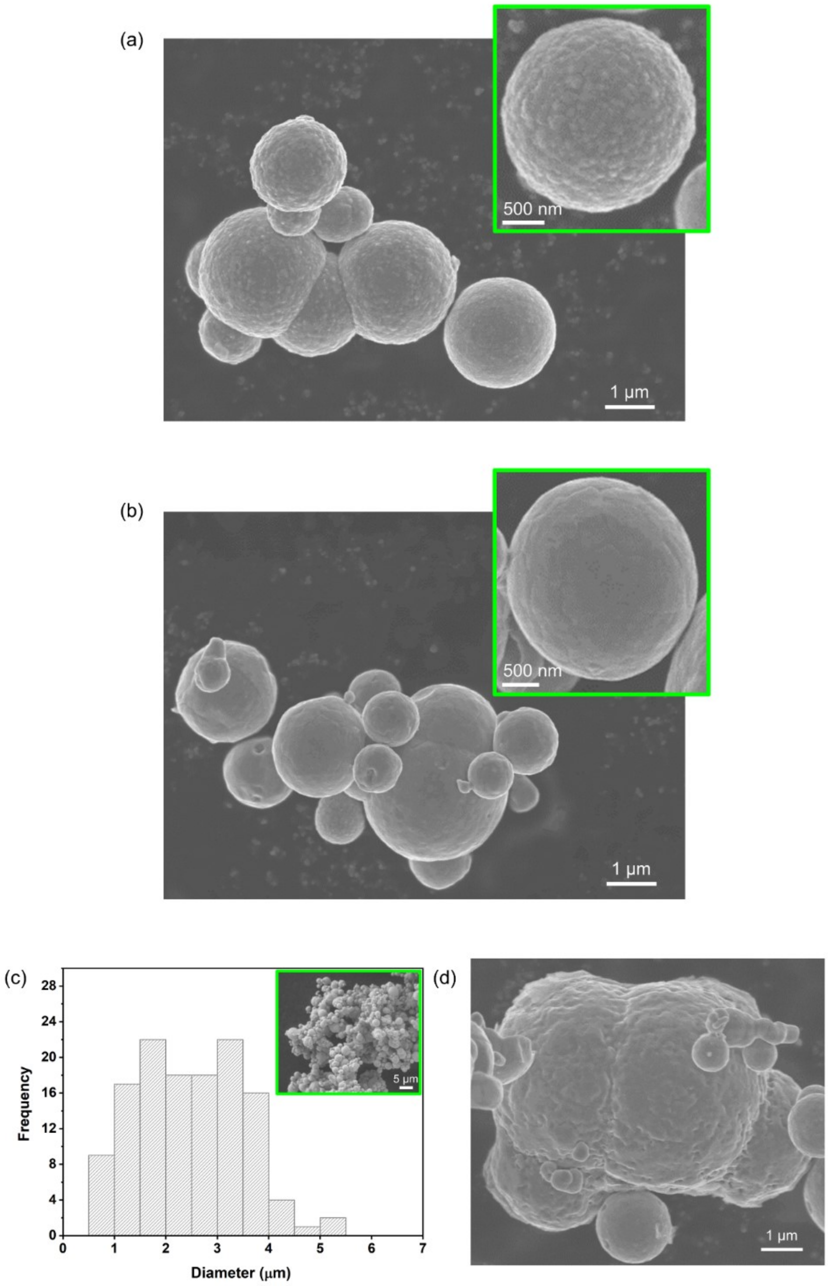

Figure SI-3: SEM images of (a) Fe particles, (b) SMPs. (c) Size distribution of the SMPs and SEM picture of the SMPs. (d) SEM of an aggregate of SMPs.

According to the SEM images (Figure SI-3 a and b) of the bare (Fe) and chemically modified (SMPs) particles, the roughness texture of the surface of the bare Fe changed to a smooth texture in the SMPs, proving the successful long chain hydrocarbon coating on the particles. As depicted in the Figure SI-3c, the SMPs size distribution is in the 0.7 - 5.5 µm range, with the higher percentage in the 1 - 4 µm range. Moreover, some aggregation of particles can be seen in Figure SI-3d.

SI-3 Stability of the SMPs under different pH solutions.

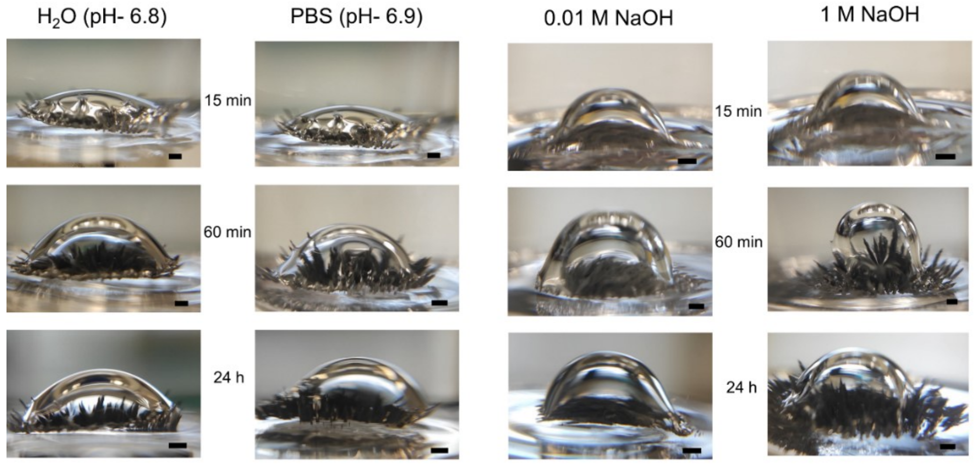

Figure SI-4: Superaerophilic stability of the SMPs under water, PBS solution, alkaline solutions of 0.01 M (pH ~ 12.1) and 1 M (pH ~ 13.9) NaOH. The particles were discharged to the surface of the water by removing the magnetic field in each solution after 15 min, 60 min and 24 h. Then, they were re-submerged inside the solution under the magnetic field followed by the loading of air volumes of 20, 40, 40 and 40 μL respectively, to demonstrate their superaerophilicity. Scale bar: 1 mm.

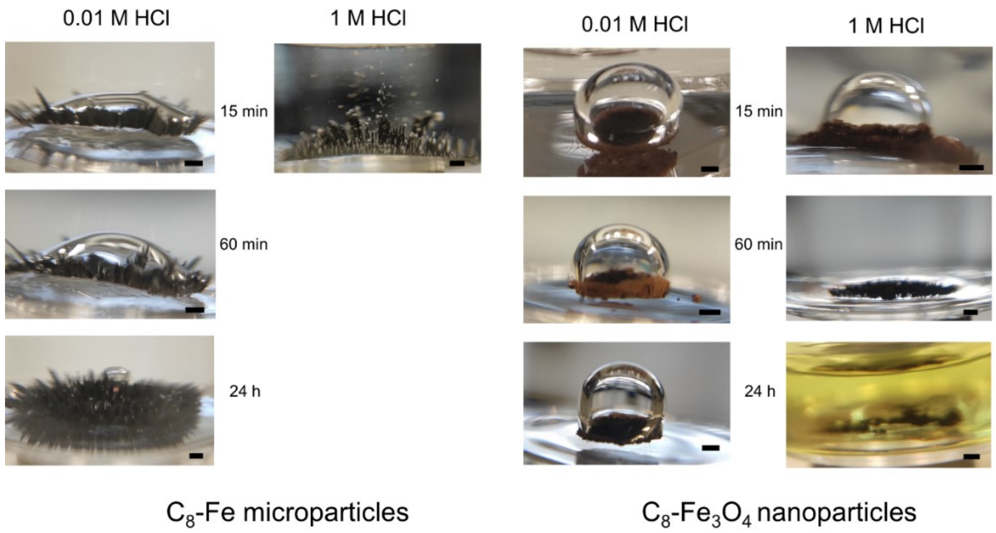

Figure SI-5: Superaerophilic stability of the SMPs (C_8-Fe microparticles) and the SMNPs (C_8-Fe_3O_4 nanoparticles) under acidic solutions of 0.01 M (pH ~ 2.1) and 1 M (pH ~ 0.2) HCl. The particles were discharged to the surface of the water by removing the magnetic field in each solution after 15 min, 60 min, and 24 h. Then, they were re-submerged inside the solution under the magnetic field followed by the loading of air volumes of 20, 40, 40 and 40 μL respectively, to demonstrate their superaerophilicity. Scale bar: 1 mm.

SI-4 Air bubble leaving behaviour under different magnetic fields

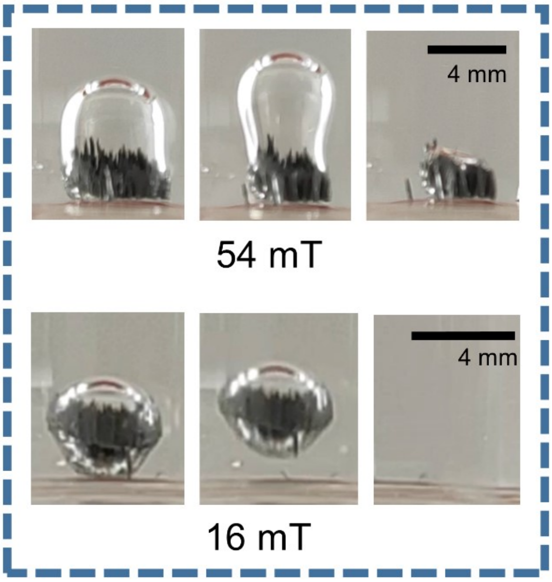

Figure SI-6: (a) 60 μL air bubble leaving the SMPs (4.0 mg) at 54 mT magnetic field (MF). (b) 10 μL air bubble leaving the glass surface together with the SMPs (4.0 mg) at 16 mT.

SI-5 Effect of different particles

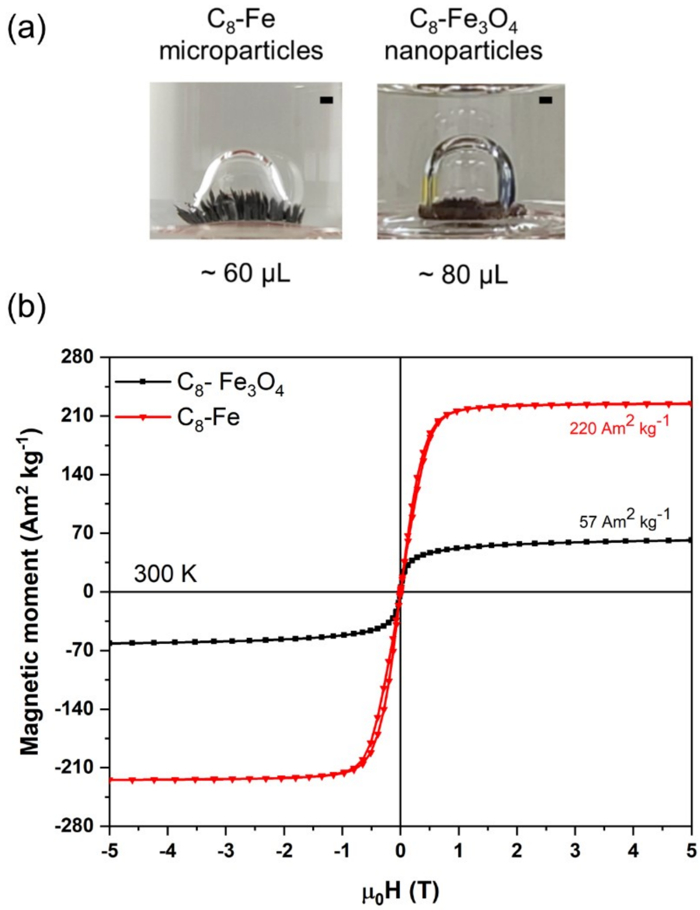

Figure SI-7: (a) Air loading capacity of 4.0 mg SMPs (C_8-Fe) and SMNPs (C_8-Fe_3O_4) under 353 mT (MF value on the glass vial surface) gradient magnetic field. (b) SQUID analysis of the SMPs and SMNPs.

SI-6 Translocation of the air bubble under different magnetic fields

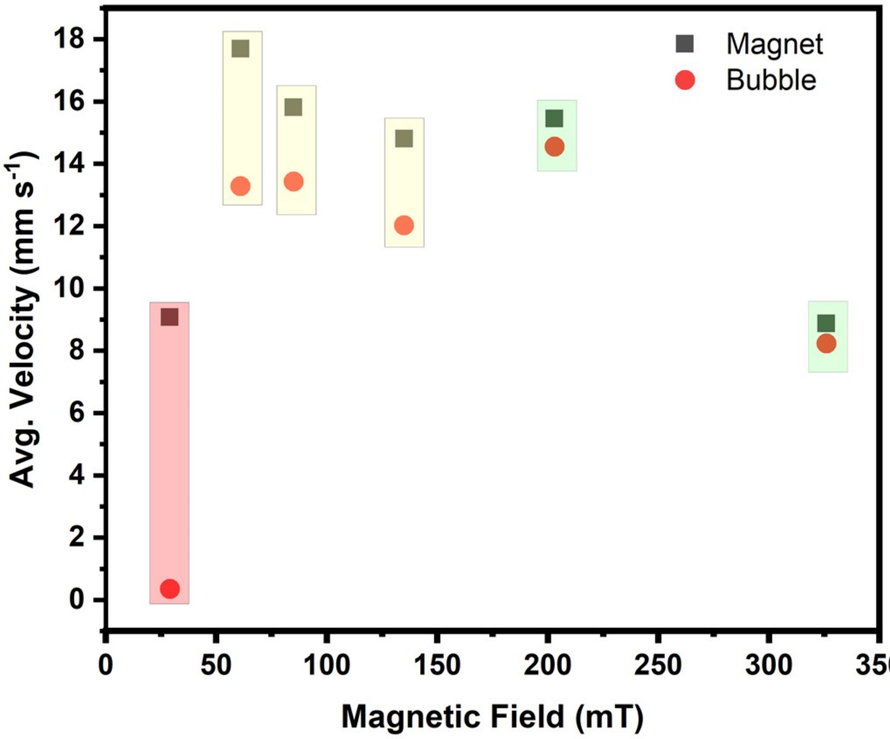

Figure SI-8: Synchronisation of the magnet and the air bubble (38 μL) under different magnetic fields.

SI-7 Trap and translocation of the air bubbles on PDMS surface.

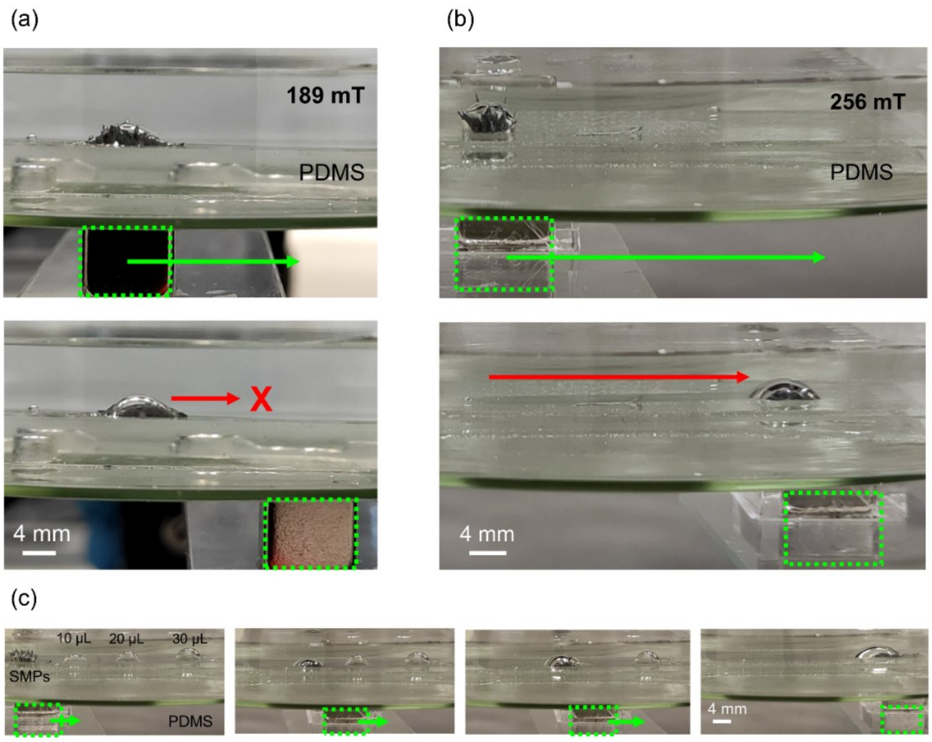

Figure SI-9: Transport of an air bubble settled in a PDMS surface under magnetic field. (a) De-bubbler did not move after magnet translocation due to the low magnetic field, 189 mT. (b) De-bubbler moved with magnet translocation due to the higher magnetic field, 256 mT. (c) Collection of deposited air bubbles of 0, 20 and 30 μL. Magnetic translocation of the bubbles under a 256 mT gradient magnetic field. Translocation of the magnet and the bubble are shown in green and red colours, respectively.

Video SI-1: Underwater air bubble transportation on PMMA surface.

Video SI-2: Underwater air bubble merging and collection on PMMA surface.

Video SI-3: Removal of a single air bubble in PMMA microfluidics channel.

Video SI-4: Removal of multiple air bubbles in PMMA microfluidics channel.

References

1 J. Wang, G. Meng, K. Tao, M. Feng, X. Zhao, Z. Li, H. Xu, D. Xia and J. R. Lu, *PLoS One*, 2012, **7**, e43478.

2 E. Herth, R. Zeggari, J. Y. Rauch, F. Remy-Martin and W. Boireau, *Microelectron. Eng.*, 2016, **163**, 43–48.

3 U. B. Gunatilake, R. Morales, L. Basabe-Desmonts and F. Benito-Lopez, *Langmuir*, 2022, **38**, 3360–3369.

4 S. Devouge, J. Conti, A. Goldsztein, E. Gosselin, A. Brans, M. Voué, J. De Coninck, F. Homblé, E. Goormaghtigh and J. Marchand-Brynaert, *J. Colloid Interface Sci.*, 2009, **332**, 408–415.